

## ORIGINAL ARTICLE

## Minor clone provides a reservoir for relapse in multiple myeloma

F Magrangeas<sup>1,2</sup>, H Avet-Loiseau<sup>2</sup>, W Gouraud<sup>1,3</sup>, L Lodé<sup>2</sup>, O Decaux<sup>1,4</sup>, P Godmer<sup>5</sup>, L Garderet<sup>6</sup>, L Voillat<sup>7</sup>, T Facon<sup>8</sup>, AM Stoppa<sup>9</sup>, G Marit<sup>10</sup>, C Hulin<sup>11</sup>, P Casassus<sup>12</sup>, M Tiab<sup>13</sup>, E Voog<sup>14</sup>, E Randriamalala<sup>15</sup>, KC Anderson<sup>16</sup>, P Moreau<sup>1,2</sup>, NC Munshi<sup>16,17</sup> and S Minvielle<sup>1,2</sup>

Recent studies have provided direct evidence for genetic variegation in subclones for various cancer types. However, little is known about subclonal evolutionary processes according to treatment and subsequent relapse in multiple myeloma (MM). This issue was addressed in a cohort of 24 MM patients treated either with conventional chemotherapy or with the proteasome inhibitor, bortezomib. As MM is a highly heterogeneous disease associated with a large number of chromosomal abnormalities, a subset of secondary genetic events that seem to reflect progression, 1q21 gain, NF- $\kappa$ B-activating mutations, *RB1* and *TP53* deletions, was examined. By using high-resolution single-nucleotide polymorphism arrays, subclones were identified with nonlinear complex evolutionary histories. Such reordering of the spectrum of genetic lesions, identified in a third of MM patients during therapy, is likely to reflect the selection of genetically distinct subclones, not initially competitive against the dominant population but which survived chemotherapy, thrived and acquired new anomalies. In addition, the emergence of minor subclones at relapse appeared to be significantly associated with bortezomib treatment. These data support the idea that new strategies for future clinical trials in MM should combine targeted therapy and subpopulations' control to eradicate all myeloma subclones in order to obtain long-term remission.

*Leukemia* (2013) 27, 473–481; doi:10.1038/leu.2012.226

**Keywords:** multiple myeloma; genomic analysis; nonlinear evolution

## INTRODUCTION

Multiple myeloma (MM) is a highly heterogeneous disease at presentation, which impacts response intensities among homogeneously treated patients. Considerable progress has, however, been achieved in the treatment of MM in the past decade, with survival improvement in newly diagnosed MM patients after the introduction of novel effective drugs, such as the immunomodulatory compound thalidomide, its analog, lenalidomide and the proteasome inhibitor, bortezomib.<sup>1–5</sup> Yet, almost all MM patients still relapse after treatment, which emphasizes a need for new insights into relapse mechanisms. Among current hypotheses, that of a composite disease with competing subclones at diagnosis and the emergence at relapse of initially minor populations is being increasingly acknowledged and supported.<sup>6</sup> In this study, the question investigated was whether such dynamics of subclonal diversification and evolution could contribute to relapse in MM. In newly diagnosed MM patients, there is a large diversity of clonal evolution stages<sup>7</sup> as well as contrasted numbers of chromosomal abnormalities.<sup>8,9</sup> This study therefore focused on the investigation of copy number changes and/or loss of heterozygosity (LOH) involving secondary genetic events associated with MM relapse such as 1q21 gain, NF- $\kappa$ B-activating mutations, *RB1* and *TP53* deletions, through the comparison of paired MM diagnosis and relapse samples.

## MATERIALS AND METHODS

## Patients and samples

Paired bone marrow (BM) samples collected at both diagnosis and relapse/progression from 24 patients initially treated in the Intergroupe Francophone du Myélome (IFM) centers either with bortezomib and dexamethasone (Vel/D) or with conventional chemotherapy (VAD: vincristine, adriamycin and dexamethasone) were included in this study (Supplementary Table 1). They were 17 males and 7 females, with a median age of 59 years (range 33–68). The median duration of remission was 24.5 months (range 4–90). Peripheral blood (PB) was also collected at relapse for 17 out of the 24 patients.

The requirements of the Declaration of Helsinki were fulfilled for all cases.

## Sample preparation

BM and PB specimens (3 ml) were obtained during standard diagnostic and follow-up procedures in IFM centers, collected on EDTA and shipped overnight to the Hematology Laboratory at University Hospital in Nantes (France). Plasma cell purification was performed as previously described.<sup>10</sup> The mean CD138<sup>+</sup> plasma cell purity was 98.1% (median 98.5; range 85–100) and 98.4% (median 99.0; range 92–100) for diagnosis and relapse samples, respectively. Aliquots of purified malignant plasma cells (500 000 cells) were frozen at –80 °C in lysis buffer (RLT+ Qiagen, Valencia, CA, USA).

<sup>1</sup>INSERM UMR 892, CNRS UMR 6299, Université de Nantes, Nantes, France; <sup>2</sup>Centre Hospitalier Universitaire, Nantes, France; <sup>3</sup>Institut de Cancérologie de l'Ouest, Nantes-Saint Herblain, France; <sup>4</sup>Centre Hospitalier Universitaire, Rennes, France; <sup>5</sup>Centre Hospitalier, Vannes, France; <sup>6</sup>Hôpital St-Antoine, Paris, France; <sup>7</sup>Centre Hospitalier, Châlons, France; <sup>8</sup>Centre Hospitalier Universitaire, Lille, France; <sup>9</sup>Institut Paoli-Calmettes, Marseille, France; <sup>10</sup>Centre Hospitalier Universitaire, Bordeaux, France; <sup>11</sup>Centre Hospitalier Universitaire, Nancy, France; <sup>12</sup>Hôpital Avicenne, Bobigny, France; <sup>13</sup>Centre Hospitalier, La Roche-sur-Yon, France; <sup>14</sup>Centre Jean Bernard, Le Mans, France; <sup>15</sup>Centre Hospitalier la Milétrie, Poitiers, France; <sup>16</sup>Leebow Institute of Myeloma Therapeutics and Jerome Lipper Multiple Myeloma Disease Center, Dana-Farber Cancer Harvard Medical School, Boston, MA, USA and <sup>17</sup>Boston VA Healthcare System, West Roxbury, Boston, MA, USA. Correspondence: Dr S Minvielle, INSERM UMR 892, CNRS UMR 6299, Université de Nantes and Centre Hospitalier Universitaire de Nantes, Unité Mixte de Génomique du Cancer, Institut de Recherche Thérapeutique de l'Université de Nantes (IRT-UN), 8 quai Moncousu—BP 70721 44007 Nantes Cedex 01, France.

E-mail: stephane.minvielle@inserm.fr

Received 11 June 2012; revised 30 July 2012; accepted 31 July 2012; accepted article preview online 9 August 2012; advance online publication, 11 September 2012

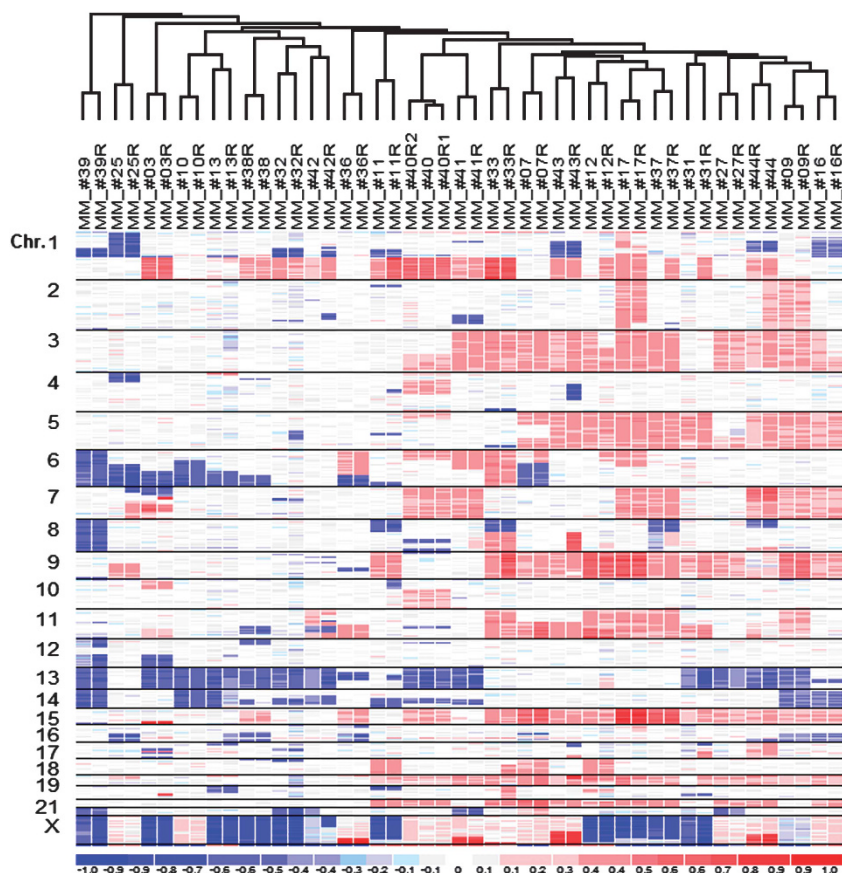


**Figure 1.** Hierarchical clustering of diagnosis and relapse MM established by SNP array data. Each case is represented by two columns for diagnosis and relapse (R). dChip median-smoothed  $\log_2$  ratio Affymetrix SNP 6.0 copy number data are arranged from 1p(tel) to Xq(tel) from top to bottom. Unsupervised hierarchical clustering of copy number data showed coclustering of all paired diagnostic and relapse samples examined. Deletions are in blue and amplifications in red. Chr., chromosome.

### Nucleic acid purification

After thawing, DNA and RNA were extracted from one aliquot using the AllPrep DNA/RNA MiniKit (Qiagen) in accordance with the manufacturers' instructions. DNA and RNA quality and quantity were assessed using the Nanodrop Spectrophotometer (NanoDrop Technologies Inc., Wilmington, DE, USA). RNA integrity was assessed using Agilent 2100 Bioanalyzer (Agilent, Palo Alto, CA, USA). For germline studies, genomic DNA was extracted from buffy coats prepared from 1 ml of PB samples using GE Healthcare Nucleon BACC Genomic DNA Extraction kits (GE Healthcare Bio-Sciences Corp., Piscataway, NJ, USA).

### Genomic analysis

DNA copy number and LOH analyses were performed on 24 diagnosis–relapse-paired BM MM samples and 17 PB/germline samples. DNA (500 ng) was processed and hybridized to Affymetrix Genome-Wide Human SNP Array 6.0 according to the manufacturer's instructions (Affymetrix, Santa Clara, CA, USA), with the exception of one diagnostic MM sample (#24) hybridized onto Affymetrix Human SNP 500K array.

Affymetrix CEL files were analyzed using Affymetrix Genotyping Console software v4.0 (GTC 4.0) for initial quality control, followed by use of the Affymetrix Birdseed algorithm v2.0 to generate single-nucleotide polymorphism (SNP) genotype calls. Genotyping using the Birdseed algorithm was performed using at least 44 arrays in each analysis. Call rates were between 97.3 and 99.74 with a mean call rate of 98.96. For MM sample #24, SNP genotype calls were generated using the BRLMM algorithm in GTC 4.0 (SNP call: 98.65 for NSP and 98.01 for STY). All samples passed the Affymetrix recommended contrast QC and SNP call rates threshold.

Copy number and LOH determinations were performed on CEL files using both Partek Genomic Suite software, version 6.5, build 6.10.0212 (Partek Inc., St Louis, MO, USA; <http://www.partek.com/>) and Affymetrix (GTC 4.0) using

software with default parameters. Baseline data were generated on paired blood DNA or International HapMap samples. The profiles were visualized with Partek Genomic Suite or Affymetrix Chromosome Analysis Suite software (ChAS v1.0.1) according to the initial analysis. Sample copy number heatmap displays were obtained from CEL files through use of the freely available dChip software (<http://www.dchip.org>) adapted to a 64-bit operating system environment.<sup>11</sup>

### Accession codes

Minimum information about a microarray experiment–compliant data have been deposited at Gene Expression Omnibus with accession number GSE37459.

### Clustering analysis

Clustering analysis was performed using dChip software based on the Pearson's correlation coefficient of  $\log_2$  ratio copy number data.

### Segmentation analysis

The detection and determination of three types of genomic events, respectively, gains, losses and copy neutral-LOH (CN-LOH) was performed using the BRLMM-P+ algorithm in GTC 4.0. To locate segments with copy number or LOH changes in CNCHP data files, Affymetrix ChAS software was used. Segmentation results were smoothed and filtered to use only segments >200 kb for gain or loss, and >4000 kb for CN-LOH. For detection of biallelic deletions the cutoff used was >50 kb.

To systematically identify genomic lesions including copy number abnormalities, LOH and minor clones present at diagnosis and at relapse, a sequential visual analysis was performed for each sample. First, copy number abnormalities (CNAs) and CN-LOH segments identified according to ChAS filters were manually curated compared with germline DNA or

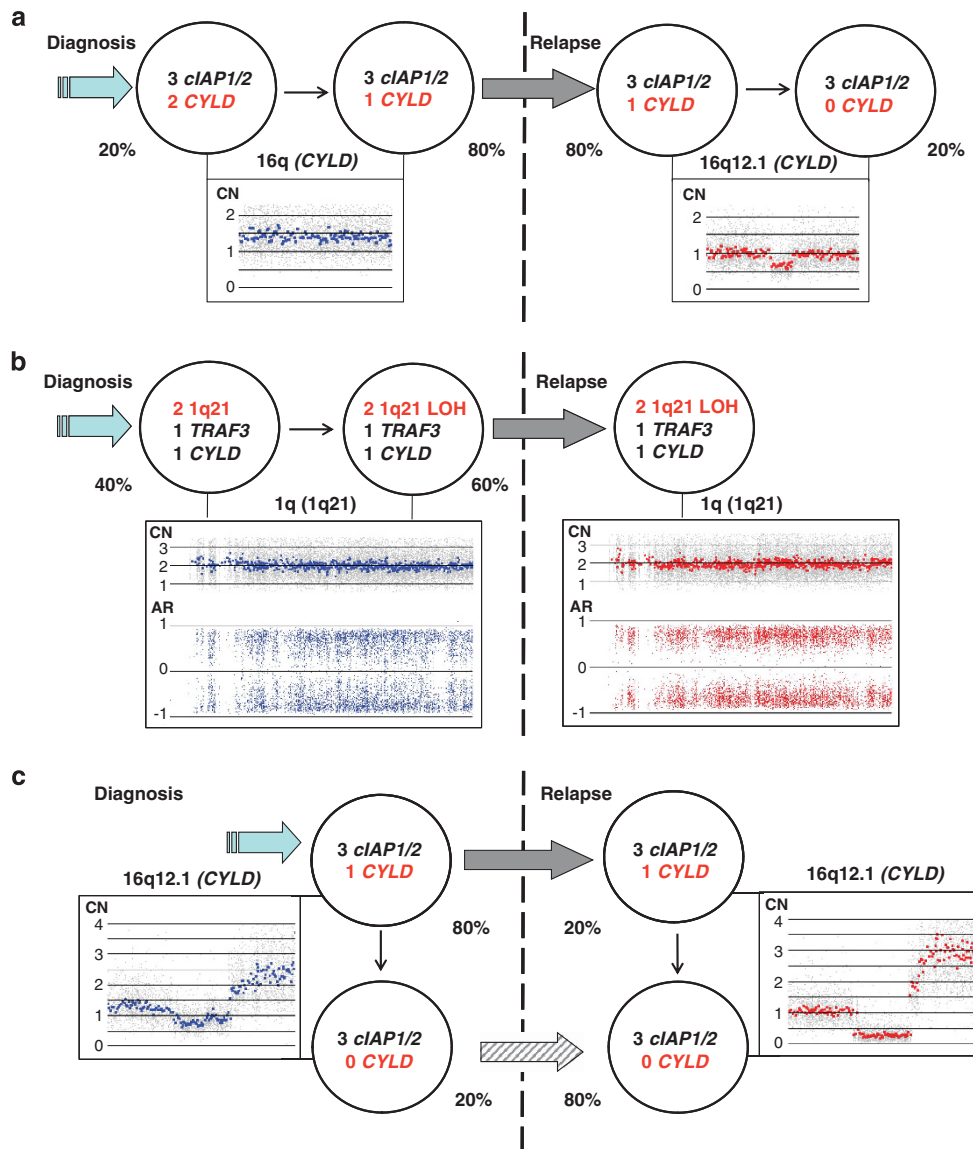


**Figure 2.** Linear subclonal evolution in MM. Examples of relapse clones originating from the major subclone at diagnosis. The proportions of subclones inferred from SNP array data at diagnostic versus relapse are indicated. Top rows (dots) display the copy number (CN) defined as the median-smoothed intensity with a window of five markers for diagnosis (blue) and relapse (red); bottom rows display allele ratios (AR) for each SNP. **(a)** Monoallelic deletion of *CYLD* at diagnosis. CN between 1.5 and 1 indicates two subclones: one deleted (80% of the population) and the other diploid (20%) (Supplementary Figure 1). Biallelic deletion of *CYLD* at relapse. CN between 1 and 0.5 indicates that the probable subclone that gave rise to relapse (80% of the population) continues to diversify and acquired a *CYLD* biallelic deletion in a minor subclone (patient no. 36). **(b)** 1q LOH without CN changes at diagnosis. AR displays a large heterozygote track indicating two subclones: one homozygous (60%) and the other heterozygous (40%) (Supplementary Figure 2). Allelic imbalance of 1q at relapse. Allele ratio shifts to a two allele track combination (homozygous SNPs cluster at ratios around -1 and 1) (patient no. 16). **(c)** *CYLD* biallelic deletion at diagnosis. CN between 1 and 0.5 indicates a *CYLD* biallelic deletion in a minor subclone. At relapse, *CYLD* biallelic deletion is predominant (CN between 0.5 and 0) (patient no. 7; other linear evolutions for patients no. 12, 13, 31, 32 and 43 are depicted in Supplementary Figure 6). Secondary genetic lesions with changes between diagnosis and relapse are indicated in red.

pooled unpaired germline samples to exclude inherited copy number variants and segments arising from experimental artifact (for example, interbatch effects). Second, segment results were compared with  $\log_2$  ratio, total copy number state and allele difference results. In case of discrepancies between these parameters, smoothing window size and segment filters were changed. Third, abnormalities present in minor clones undetected by segmentation analysis were identified using total copy number and allele-specific copy number estimates obtained using Partek Genomic Suite analysis as well as allele difference and  $\log_2$  ratio obtained by GTC 4.0 analysis to manually define emerging segments. The Genomic Segmentation algorithm of Partek Genomic Suite for Genome-Wide Human SNP Array 6.0 was used to validate segmentation analysis results.

DNA gains and losses arising from B-cell receptor gene rearrangements at 2p11.2 (IGK@), 14q32.33 (IGH@) and 22q11.22 (IGL@) were excluded from the analysis.

#### Detection of minor populations and assessment of relative frequencies of subclones

A visual reference was constructed for each lesion type (gain, loss or CN-LOH) based on spiking increased amount of tumoral DNA harboring the lesion in matched germline DNA (Supplementary Figures 1–3). This scale, based on total copy number, allele ratio and allele-specific copy number determinations, was used to estimate the proportion of MM clones

harboring a specific lesion within myeloma cells lacking this abnormality. The detection threshold of a minor subclone was established at 20%.

### Breakpoint analyses

Based on decreased microarray signal intensities, primers flanking the predicted deletions were designed using Primer3<sup>12</sup> (MM\_#11: P11 5\_1 5'-TT GCCTGTGGACTGTCAGCTCTGTG-3', P11 3\_1 5'-GCTCCTGGTTCACACAGCCC CTATC-3'; MM\_#42: P42 5\_1 5'-GCCAAATCATTCCAGCCTGAGGAA-3', P42 3\_3 5'-CAGGAGACCACTGCAGGAAAGACTCA-3'). PCR was performed on relapse samples using 100 ng genomic DNA in accordance with the manufacturers' instructions (Advantage 2 PCR Kit, Clontech, Mountain View, CA, USA) with the following thermal program: 1-min initial denaturation at 95 °C; 35 cycles of 30 s at 95 °C and 3 min at 68 °C followed by a 3-min final extension step at 68 °C. Genomic deletion

breakpoints were defined by direct sequencing of PCR products. PCR genotyping across breakpoints was then performed on DNA from BM diagnosis samples either with initial primers (MM\_#11) or primers designed by sequencing of the deletion breakpoints (MM\_#42: P42 5\_S 5'-CAGTCCC TGAACCTCACTCCTCACG-3', P42 3\_3). DNA from a PB sample of patient MM\_#42 at relapse was also tested.

### Gene set enrichment analysis

MM samples for which 50 ng of total RNA from diagnosis and relapse samples was available (11 cases) were processed according to NuGEN manufacturer's instruction (NuGEN, San Carlos, CA, USA) before labeling and hybridization onto Affymetrix Human Exon1.0 chip according to the manufacturer's instructions (Affymetrix). For each gene of interest, Spearman's correlation coefficient ( $\rho$ ) was computed between the

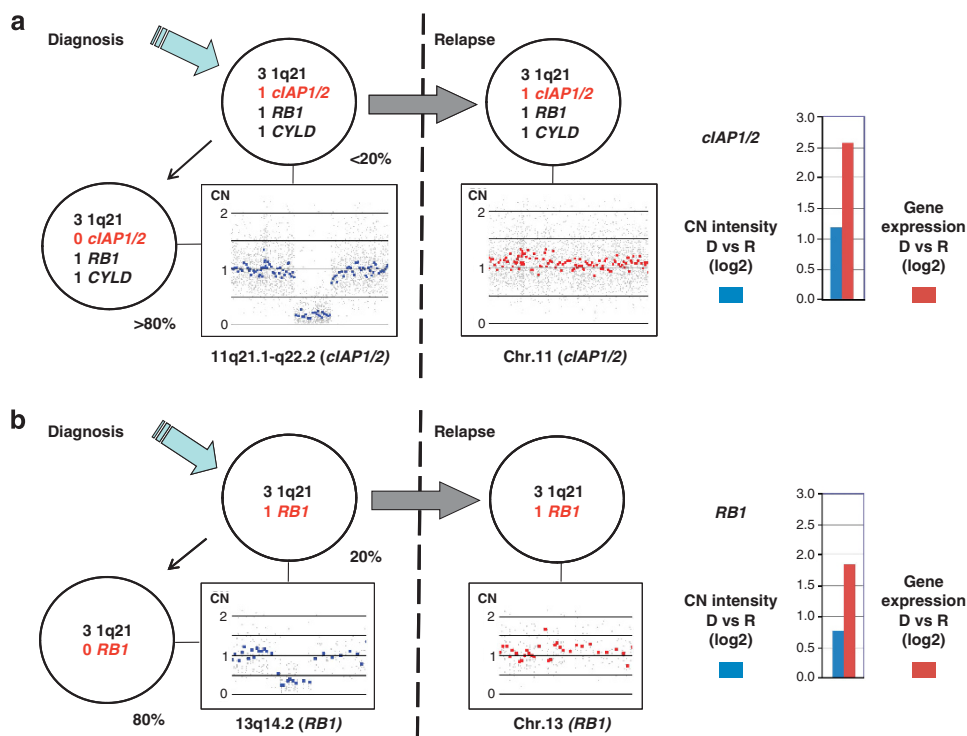


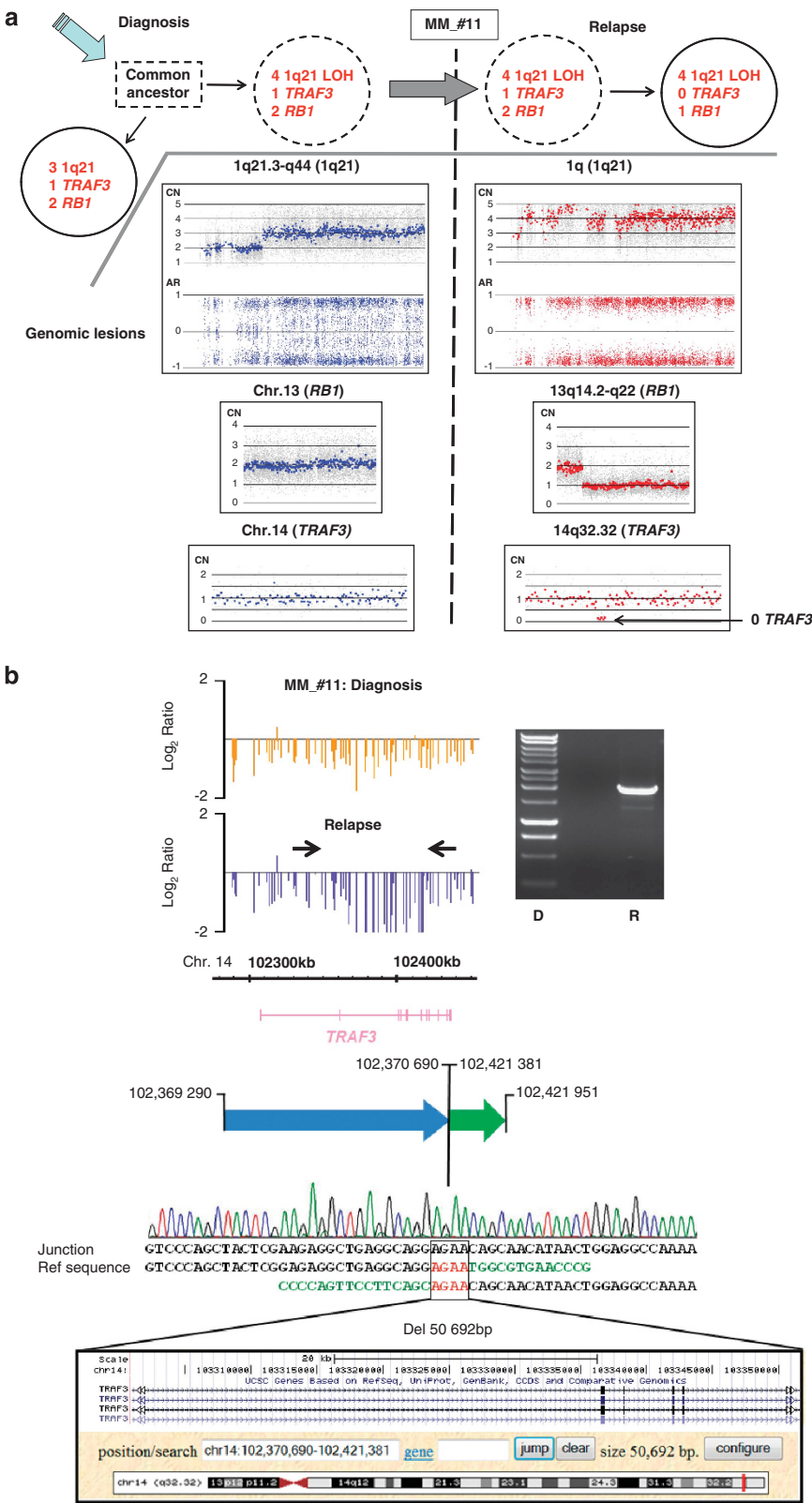
**Figure 3.** Nonlinear subclonal evolution in MM. Examples of relapse clones originating from a minor subclone present at diagnosis with bifurcation in clonal evolution. Proportions of subclones inferred from SNP array data on diagnosis versus relapse are indicated. Rows (dots) display the copy number (CN) defined as the median-smoothed intensity with a window of five markers at diagnosis (blue) and relapse (red). Right inserts show the correspondence between CN intensity changes and gene expression changes. (a) Biallelic deletion of *c1AP1/2* at diagnosis; CN near 0 indicates a predominant subclone with *c1AP1/2* biallelic deletion and a very minor subclone with *c1AP1/2* monoallelic deletion. Monoallelic deletion of *c1AP1/2* at relapse; CN at 1 indicates that the most likely subclone that gave rise to relapse had one copy of Chr.11 (patient no. 38). (b) Biallelic deletion of *RB1* at diagnosis; CN < 0.5 indicates one major subclone with *RB1* biallelic deletion and a minor subclone with *RB1* monoallelic deletion. Monoallelic deletion of *RB1* at relapse. CN at 1 indicates that the probable subclone that gave rise to relapse had one copy of *RB1* (patient no. 41). Secondary genetic lesions with changes between diagnosis and relapse are indicated in red; D, diagnosis, R, relapse. Chr., chromosome.

**Figure 4.** Nonlinear subclonal evolution with new acquisitions at relapse in patient no. 11. (a) Relapse clone originating from minor subclone at diagnosis with bifurcation and diversification. Rows (dots) display the copy number (CN) defined as the median-smoothed intensity with a window of five markers of diagnosis (blue) and relapse (red), bottom rows display allele ratio (AR) for each SNP. 1q21.3-q44 gain at diagnosis; CN at 3 indicates one predominant subclone. At relapse: 1q gain LOH; CN at 4 and AR with a two allele track combination (homozygous SNPs cluster at ratios around -1 and 1) indicate that the most likely subclone that gave rise to relapse had 1q gain LOH undetectable at diagnosis. Acquisition of del13q14-q22 and biallelic deletion of *TRAF3* at relapse. Dashed circle indicates that the frequency of this subclone is too low (<20%) to be detected. Secondary genetic lesions with changes between diagnostic and relapse are indicated in red. (b) Genomic pattern of *TRAF3* rearrangements acquired at relapse. Top left, genomic map showing position and log<sub>2</sub> ratio copy number of array probes as individual vertical line (orange for diagnosis and blue for relapse) and region of deletion, black arrows indicate PCR primers location; right, PCR genotyping across breakpoints at diagnosis and relapse, a breakpoint-specific PCR product corresponding to *TRAF3* deletion was detected only at relapse indicating that this rearrangement was acquired at relapse. Bottom, sequence of the PCR product spanning the breakpoint junction of the deletion; letters in green indicate nucleotides deleted and letters in red indicate identical sequences at the site of the breakpoint. Dashed circle indicates that the frequency of this subclone is too low (<20%) to be detected. Deletion in *TRAF3* removes four coding exons. D, diagnosis; R, relapse. Chr., chromosome.



corresponding probeset of the Affymetrix U133Plus2 array and each of the corresponding probesets of the Affymetrix Human Exon 1.0 ST (exon extended analysis), based on a cohort of nine patients analyzed using both arrays. Only correlation coefficients above 70 were considered (102 090 probes). If none of a probeset correlation coefficient of a gene symbol was above 0.70, then the best (nearest to 0.70) probeset was kept (6394

probes). Data were analyzed at the gene level with Expression Console Affymetrix software v1.1 using RMA algorithm. Gene set enrichment analyses<sup>13</sup> were carried out to determine whether defined sets of genes within a collection of 2457 gene sets showed statistically significant, concordant differential expression in MM samples at diagnosis versus relapse.

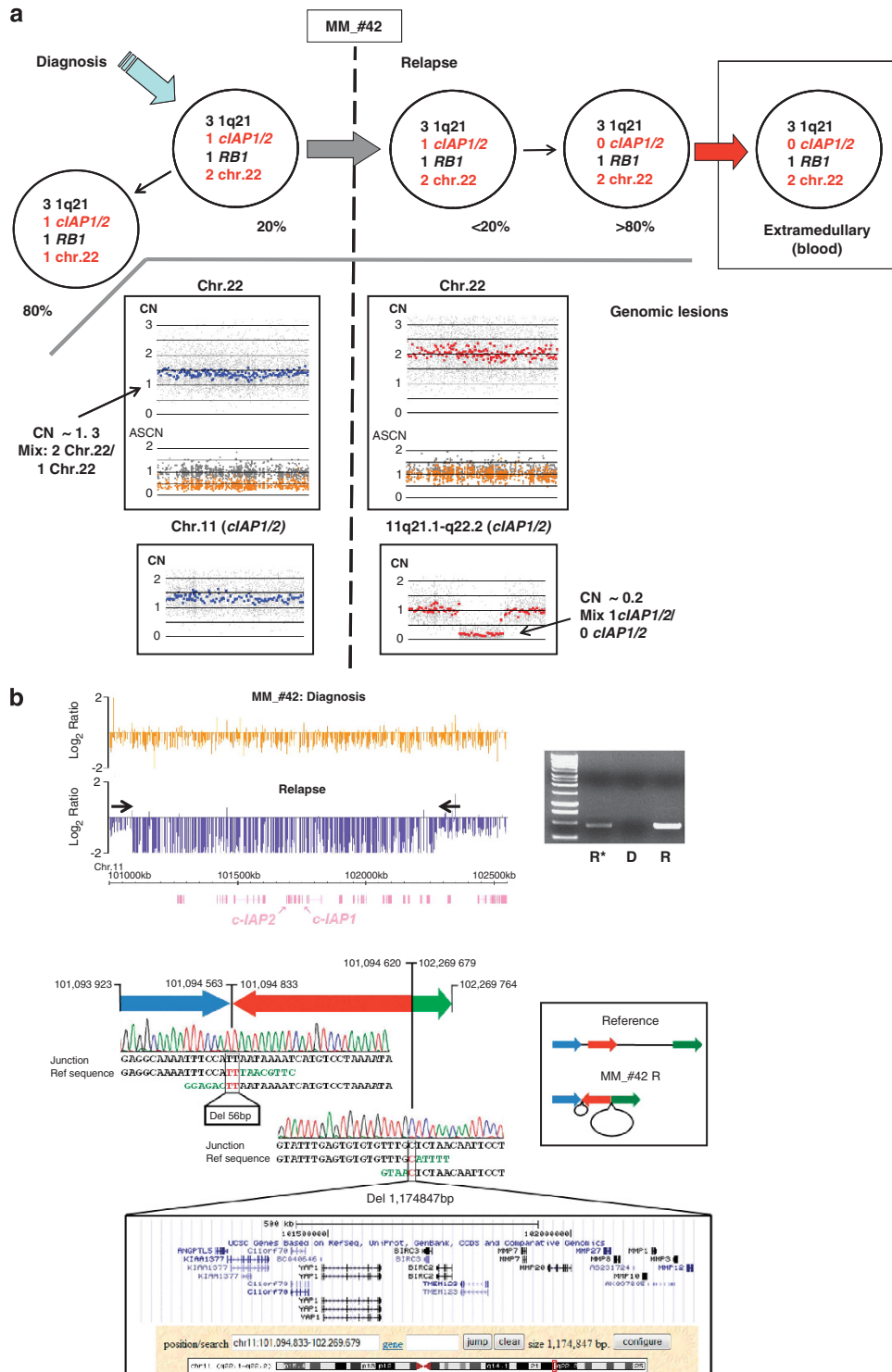


## RESULTS

## Genomic lesions in matched diagnostic and relapse MM samples

Genomic analyses were first performed by integrating total copy number, allele-specific copy number and allele ratio calculations obtained using high-resolution SNP arrays. This analysis revealed a complex genomic landscape of chromosomal abnormalities at diagnosis with a large number of diverse CNAs and LOH. Overall genomic analysis identified a mean of 15.8 CNAs per MM case at

diagnosis, gains and losses being equally represented and a mean of 2.0 CN-LOH (Supplementary Tables 2 to 5). Despite interpatient disparity, all MM genomic hallmarks were represented, that is, del13, hyperdiploidy and 1q21 gain in 67, 50 and 50% of the cases, respectively. Biallelic deletions were also detected, targeting *TRAF3*, *clAP1/2*, *CYLD* and *RB1* (Supplementary Table 6). Relapse was associated with a significant increase to 19.1 in the mean number of CNAs per case ( $P < 0.001$ ). Acquisitions involved predominantly lesions described as secondary genetic events,<sup>7</sup> that is, 1q21 gain (five cases), NF- $\kappa$ B-activating mutations (five



cases) and *TP53* deletion (two cases). Lesions present at diagnosis were lost in 10 (42%) cases at relapse (Supplementary Table 6). In addition, changes in the proportions of myeloma cell populations harboring subclones present at diagnosis were identified in five cases (Supplementary Table 6). For example, in patient #39, a minor subpopulation with a biallelic deletion targeting *AJAP1* at diagnosis became predominant at relapse (Supplementary Figure 4). These results suggest that, at least in some patients, a complex clonal evolutionary process occurs during disease progression.

#### Clonal relationships between matched diagnostic and relapse MM samples

Unsupervised clustering analysis using SNP array data indicated a clear clonal relationship between all matched diagnostic and relapse MM samples (Figure 1). The pattern of deletions at immunoglobulin gene loci confirmed a common clonal origin, although rearrangement-associated deletions across all loci were highly variable between individual MM cases (Supplementary Figure 5). These data strongly suggested that relapse represented intraclonal evolution and diversification of the myeloma cell population present at diagnosis.

#### Nonlinear evolution in MM patients at relapse

The marked genetic heterogeneity among patients and dominating subclones at diagnosis, combined with the diversity of changes at relapse, prompted to focus the study on a limited number of recurrent secondary genetic events. In the 24 cases, seven genomic lesions were scrutinized, respectively, involving the 1q21 locus, NF- $\kappa$ B pathway regulators *TRAF3*, *CIAP1/2*, *CYLD* and *CD40* as well as *RB1* and *TP53* tumor suppressor genes. Reporting each lesion based on SNP array analysis allowed to identify a genetic profile for each patient and establish the relative abundance of genetically distinct subclones at the respective time points of diagnosis and relapse (Supplementary Figures 1–3). From these comparisons, it was therefore possible to infer for each patient whether the relapse had a clonal origin, assuming that the acquisition of a genomic lesion (CNAs or CN-LOH) is irreversible and therefore drives changes unidirectionally by sequential acquisition of one or more events. Three equivalent patterns emerged from this analysis, with eight patients in each group. For a first third of the cases, there were no differences between diagnostic and relapse clones. For another third, the relapse clone apparently derived from the major subclone at diagnosis but continued to diversify through additionally acquired lesions (Figures 2a and b), although it cannot be excluded that more than one subclone had contributed to relapse (Figure 2c). For the

final third of patients, the relapse clone clearly derived from a minor subclone, barely present at diagnosis. For example, dominant subclones at diagnosis with biallelic deletion of *CIAP1/2* (MM patient #38; Figure 3a) or biallelic deletion of *RB1* (MM patient #41; Figure 3b) were absent at relapse. This indicates that a preexisting minor subclone blossomed at relapse. As a consequence, in both of these cases, selection of the minor clone lacking the relevant biallelic deletion led to a large increase of either *CIAP1/2*- or *RB1*-expressing cells at relapse. In most of the patients, the relapse clone continued to diversify by acquiring one or two secondary genetic events (MM patient #11; Figure 4) and also invaded PB (MM patient #42; Figure 5). Bifurcation in clonal evolution contra-selected subclones carrying various lesions including chromosome 17 CN-LOH, chromosome 22 deletion, chromosome 2 gain, 7q11.22-q22.11 gain and 1p22.1-p13.3 deletion (see Supplementary Figure 7). Nonlinear patterns of evolution were also observed in two patients without changes in the secondary genetic events explored (Supplementary Figure 8).

Of note, reordering of intraclonal architecture was mostly observed in patients treated with the proteasome inhibitor bortezomib rather than in patients treated with conventional chemotherapy ( $P = 0.036$ ; Supplementary Table 7).

#### Upregulation of NF- $\kappa$ B genes at relapse

Functional changes associated with the acquisition of CNAs and CN-LOH, and combined with the emergence of minor subclones at relapse. A gene set enrichment analysis was therefore performed, comparing gene expression profiles between diagnostic MM ( $n = 11$ ) and relapse MM ( $n = 12$ ). This revealed a significant difference in the expression pattern of known NF- $\kappa$ B pathway genes, notably enriched at relapse (gene set: ST\_TUMOR\_NECROSIS\_FACTOR\_PATHWAY,  $P = 0.037$ , Supplementary Table 8 and Supplementary Figure 9). Conversely, in diagnosis cases, there was an overrepresentation of downregulated genes when the NF- $\kappa$ B pathway is activated (gene set: BASSO\_CD40\_SIGNALING\_DN,  $P = 0.002$ , Supplementary Table 9). These results, together with data showing that in four patients relapse-acquired lesions targeted NF- $\kappa$ B regulators, strongly suggest that activation of this pathway could contribute to relapse mechanisms in MM.

## DISCUSSION

In this study, genomic anomalies were screened in mature tumor cells (CD138+) from MM patients. Comparison of paired diagnosis and relapse DNA samples by SNP array revealed two distinct patterns of subclonal evolution in MM in the two thirds of

**Figure 5.** Nonlinear subclonal evolution with new acquisition at relapse and extramedullary expansion in patient no. 42. Relapse clone originating from minor subclone at diagnosis with bifurcation, diversification and extramedullary expansion. Proportion of subclones inferred from SNP array data on diagnostic versus relapse are indicated. Top rows (dots) display the copy number (CN) defined as the median-smoothed intensity with a window of five markers of diagnosis (blue) and relapse (red), bottom rows display allele-specific copy number (ASCN) with minimum (orange) and maximum allele (gray) intensities. (a) Deletion of chromosome 22 at diagnosis. CN between 1.5 and 1, and minimum allele intensity  $< 0.5$  detached from the maximum allele indicate two subclones: one deleted (80% of the population) and the other diploid (20%) (Supplementary Figure 1). Normal diploid chromosome 22 at relapse; CN at 2 and ASCN shows both alleles separated with the minimum allele (orange) intensity 1 indicating that the most likely subclone that gave rise to relapse had two copies of chromosome 22. Acquisition of biallelic deletion of *CIAP1/2* at relapse. CN near 0 indicates a predominant subclone with *CIAP1/2* biallelic deletion and a very minor subclone with *CIAP1/2* monoallelic deletion. Secondary genetic lesions with changes between diagnostic and relapse are indicated in red. (b) Genomic pattern of *CIAP1/2* rearrangements acquired at relapse. Top left, genomic map showing position and  $\log_2$  ratio copy number of array probes as individual vertical line (orange for diagnosis and blue for relapse) and region of deletion, black arrows indicate PCR primers location; right, PCR genotyping across breakpoints at diagnosis and relapse, a breakpoint-specific PCR product corresponding to *CIAP1/2* locus deletion was detected only at relapse indicating that this rearrangement was acquired at relapse. Bottom, sequence of the PCR product spanning the breakpoint junction of the deletion, letters in green indicate nucleotides deleted and letters in red indicate identical sequences at the site of the breakpoint. Bottom, mapping of the genes involved in the rearrangements using UCSC Genome Browser (NCBI36/hg18). Intrachromosomal rearrangements on chromosome 11q that combine a short deletion, an inversion and a large deletion remove 16 genes including *CIAP1/2* (*BIRC2/BIRC3*). An illustration of the inverted sequence and deletions is shown on the right. Inverted sequence relative to the reference is in red; those in the same orientation are in blue and green. The black loops represent the deleted sequence. Genomic location is indicated. D, diagnosis; R, relapse; R\*, blood sample collected at relapse. Chr., chromosome.

patients with new clones at relapse. A linear pattern was disclosed, in which the major diagnosis subclone acquired additional lesions and evolved to a relapse subclone. Second, a nonlinear pattern was observed in a third of the patients, in which the dominant subclone at presentation was killed by therapy while a minor subclone survived and expanded at relapse. This nonlinear pattern was observed preferentially in patients treated with bortezomib rather than those treated with conventional induction chemotherapy, and preferably in patients who achieved complete response or very good partial response. This suggests that bortezomib-based treatment specifically extinguishes the dominant subclone carrying the 'driver' mutation of symptomatic MM, while other subclones persist, providing a reservoir for relapse. Minor subclones that are not initially competitive against the dominant population cells therefore have a chance to thrive and acquire new anomalies. The apparent difference in terms of selection pressure between pathway-oriented and conventional drugs could explain why, in the IFM 2005-01 phase III trial, the better response rate observed in patients who received bortezomib plus dexamethasone versus VAD was not fully translated into a significant longer progression-free survival.<sup>4</sup>

Intraclonal evolution diversity in the course of MM was screened here with a limited number of CNAs referred to as secondary genetic lesions, at two time points and in a small cohort of patients, with a 20% threshold for the detection of subclone frequency. For these reasons, and because of the number and variety of CNAs at diagnosis, this provided an underestimated image of the genetic evolution of MM. Moreover, mature tumor cells were selected, leaving out possible other anomalies present in earlier stages of MM maturation, such as CD138 – precursors or side population progenitors.<sup>14,15</sup>

Nevertheless, these data suggest a profound reorganization and diversification of the subclonal population with frequent nonlinear dynamics during disease progression. They also demonstrate that MM not only have multiple subclones at diagnosis but also retain the capacity to diversify through additional acquired lesions, especially in nonlinear pattern. This was particularly well illustrated with patient no. 41 and no. 42. In the latter case, the subclonal bifurcation involved at least three lesions harbored by the major subclone(s) at diagnosis. Moreover, diversification/evolution was attested by the acquisition of more than 10 new lesions at relapse, including homozygous deletions targeting *FAT3*, *MTNR1B*, *CIAP1/2* and *SLITRK1*, strongly suggesting increased genomic instability during progression. This feature was reinforced by the breakpoint signature observed at the *CIAP1/2* locus in patient no. 42, characterized by the presence of microhomology at junctions, with deletions of various lengths and inverted sequences. This is consistent with microhomology-mediated break-induced replication complex rearrangements described to be compatible with genomic instability.<sup>16–18</sup>

This study moreover confirmed the central role of constitutive NF- $\kappa$ B activation in the progression of MM and relapse.<sup>19,20</sup> This phenomenon is probably complex and may result from the combination of newly acquired activating mutations, cooperation with other pathways and/or changes in the microenvironment. However, the strong evolutionary plasticity of subclones harboring biallelic deletion of *CIAP1/2* (*BIRC2/3*) with either re-emergence, eradication or emergence of subclones described in this work and recently by Keats et al.<sup>21</sup> indicates that clonal dynamics also contributes to deregulation of the NF- $\kappa$ B pathway in myeloma patients at relapse.

While single-cell whole-genome sequencing will be ultimately required to define precisely the frequency of subclonal populations and the mutations in the founding clone evolution, these data together with those prepublished online<sup>21–23</sup> extend results obtained in other hematological malignancies.<sup>24–27</sup> Together with previous results showing subclonal heterogeneity at several stages of the disease,<sup>28–31</sup> these data support the concept of a Darwinian

model of clonal evolution in cancer,<sup>6</sup> in the context of MM progression and relapse.<sup>32</sup>

This conceptual framework has clinical implications in MM as treatment clearly appeared to affect clonal selection. In a Darwinian model of clonal evolution, the sequence of treatment (induction, consolidation and maintenance) using drugs with various modes of action, such as alkylating agents, immunomodulators and proteasome inhibitors, is therefore a crucial point to consider in order to eradicate the more aggressive subclones and control indolent subpopulations in order to obtain long-term remission. In the near future, with the advent of targeted drugs, in addition to risk stratification (based on interphase fluorescent *in situ* hybridization, gene expression profiling or SNP array,<sup>33</sup> the identification of altered pathways and allelic variant frequency at presentation could be critical to combine and sequence the usage of different drugs.

## CONFLICT OF INTEREST

The authors declare no conflict of interest.

## ACKNOWLEDGEMENTS

This study was supported by IFM; the French National Research Agency, Grant R08079NS (to SM); the French Institute National du Cancer, Grant R09076NN (to HA-L); the National Institutes of Health, Grants P01 CA155258-01 (to NCM, SM, HA-L and KCA), R01-124929 (to NCM), P50-100007 and P01-78378 (to NCM and KCA), and Department of Veterans Affairs Merit Review Awards. We thank Elise Douillard, Magali Devic, Emilie Maureton and Nathalie Roi for excellent technical expertise. We also thank Marie C Béné for critical reading of the manuscript.

## AUTHOR CONTRIBUTIONS

PM, OD, PG, LG, LV, TF, AMS, GM, CH, PC, MT, EV, ER and HA-L provided study materials or patients, and collected clinical follow-up data. FM, LL, HA-L, WG and SM analyzed the data. FM, HA-L, NCM, KCA and SM designed the study. SM and FM wrote the report. All investigators reviewed the final report.

## REFERENCES

- Barlogie B, Tricot G, Anaissie E, Shaughnessy J, Rasmussen E, van Rhee F et al. Thalidomide and hematopoietic-cell transplantation for multiple myeloma. *N Engl J Med* 2006; **354**: 1021–1030.
- Facon T, Mary JY, Hulin C, Benboubker L, Attal M, Pegourie B et al. Melphalan and prednisone plus thalidomide versus melphalan and prednisone alone or reduced-intensity autologous stem cell transplantation in elderly patients with multiple myeloma (IFM 99-06): a randomised trial. *Lancet* 2007; **370**: 1209–1218.
- San Miguel JF, Schlag R, Khuageva NK, Dimopoulos MA, Shpilberg O, Kropff M et al. Bortezomib plus melphalan and prednisone for initial treatment of multiple myeloma. *N Engl J Med* 2008; **359**: 906–917.
- Harousseau JL, Attal M, Avet-Loiseau H, Marit G, Caillot D, Mohty M et al. Bortezomib plus dexamethasone is superior to vincristine plus doxorubicin plus dexamethasone as induction treatment prior to autologous stem-cell transplantation in newly diagnosed multiple myeloma: results of the IFM 2005-01 phase III trial. *J Clin Oncol* 2010; **28**: 4621–4629.
- Rajkumar SV, Jacobus S, Callander NS, Fonseca R, Vesole DH, Williams ME et al. Lenalidomide plus high-dose dexamethasone versus lenalidomide plus low-dose dexamethasone as initial therapy for newly diagnosed multiple myeloma: an open-label randomised controlled trial. *Lancet Oncol* 2010; **11**: 29–37.
- Greaves M, Maley CC. Clonal evolution in cancer. *Nature* 2012; **481**: 306–313.
- Fonseca R, Bergsagel PL, Drach J, Shaughnessy J, Gutierrez N, Stewart AK et al. International Myeloma Working Group molecular classification of multiple myeloma: spotlight review. *Leukemia* 2009; **23**: 2210–2221.
- Walker BA, Leone PE, Jenner MW, Li C, Gonzalez D, Johnson DC et al. Integration of global SNP-based mapping and expression arrays reveals key regions, mechanisms, and genes important in the pathogenesis of multiple myeloma. *Blood* 2006; **108**: 1733–1743.
- Avet-Loiseau H, Li C, Magrangeas F, Gouraud W, Charbonnel C, Harousseau JL et al. Prognostic significance of copy-number alterations in multiple myeloma. *J Clin Oncol* 2009; **27**: 4585–4590.
- Avet-Loiseau H, Facon T, Grosbois B, Magrangeas F, Rapp MJ, Harousseau JL et al. Oncogenesis of multiple myeloma: 14q32 and 13q chromosomal abnormalities



- are not randomly distributed, but correlate with natural history, immunological features and clinical presentation. *Blood* 2002; **99**: 2185–2191.
- 11 Lin M, Wei LJ, Sellers WR, Lieberfarb M, Wong WH, Li C. dChipSNP: significance curve and clustering of SNP-array-based loss-of-heterozygosity data. *Bioinformatics* 2004; **20**: 1233–1240.
  - 12 Rozen S, Skaletsky HJ. Bioinformatics methods and protocols. In Krawetz S, Misener S (eds) *Methods in Molecular Biology*. Humana Press: Totowa, NJ, pp 365–386, 2000.
  - 13 Subramanian A, Tamayo P, Mootha VK, Mukherjee S, Ebert BL, Gillette MA *et al*. Gene set enrichment analysis: a knowledge-based approach for interpreting genome-wide expression profiles. *Proc Natl Acad Sci USA* 2005; **102**: 15545–15550.
  - 14 Matsui W, Huff CA, Wang Q, Malehorn MT, Barber J, Tanhehco Y *et al*. Characterization of clonogenic multiple myeloma cells. *Blood* 2004; **103**: 2332–2336.
  - 15 Jakubikova J, Adamia S, Kost-Alimova M, Klippel S, Cervi D, Daley JF *et al*. Lenalidomide targets clonogenic side population in multiple myeloma: pathophysiology and clinical implications. *Blood* 2011; **117**: 4409–4419.
  - 16 Hastings PJ, Ira G, Lupski JR. A microhomology-mediated break-induced replication model for the origin of human copy number variation. *PLoS Genet* 2009; **5**: e1000327.
  - 17 Hastings PJ, Lupski JR, Rosenberg SM, Ira G. Mechanisms of change in gene copy number. *Nat Rev Genet* 2009; **10**: 551–564.
  - 18 Conrad DF, Bird C, Blackburne B, Lindsay S, Mamanova L, Lee C *et al*. Mutation spectrum revealed by breakpoint sequencing of human germline CNVs. *Nat Genet* 2010; **42**: 385–391.
  - 19 Annunziata CM, Davis RE, Demchenko Y, Bellamy W, Gabrea A, Zhan F *et al*. Frequent engagement of the classical and alternative NF-kappaB pathways by diverse genetic abnormalities in multiple myeloma. *Cancer Cell* 2007; **12**: 115–130.
  - 20 Keats JJ, Fonseca R, Chesi M, Schop R, Baker A, Chng WJ *et al*. Promiscuous mutations activate the noncanonical NF-kappaB pathway in multiple myeloma. *Cancer Cell* 2007; **12**: 131–144.
  - 21 Keats JJ, Chesi M, Egan JB, Garbitt VM, Palmer SE, Braggio E *et al*. Clonal competition with alternating dominance in multiple myeloma. *Blood* 2012; **120**: 1067–1076.
  - 22 Egan JB, Shi CX, Tembe W, Christoforides A, Kurdoglu A, Sinari S *et al*. Whole genome sequencing of multiple myeloma from diagnosis to plasma cell leukemia reveals genomic initiating events, evolution and clonal tides. *Blood* 2012; **120**: 1060–1066.
  - 23 Walker BA, Wardell CP, Melchor L, Hulkki S, Potter NE, Johnson DC *et al*. Intracлонаl heterogeneity and distinct molecular mechanisms characterize the development of t(4;14) and t(11;14) myeloma. *Blood* 2012; **120**: 1077–1086.
  - 24 Mullighan CG, Phillips LA, Su X, Ma J, Miller CB, Shurtleff SA *et al*. Genomic analysis of the clonal origins of relapsed acute lymphoblastic leukemia. *Science* 2008; **322**: 1377–1380.
  - 25 Anderson K, Lutz C, van Delft FW, Bateman CM, Guo Y, Colman SM *et al*. Genetic variegation of clonal architecture and propagating cells in leukaemia. *Nature* 2011; **469**: 356–361.
  - 26 Notta F, Mullighan CG, Wang JC, Poepl A, Doulatov S, Phillips LA *et al*. Evolution of human BCR-ABL1 lymphoblastic leukaemia-initiating cells. *Nature* 2011; **469**: 362–367.
  - 27 Ding L, Ley TJ, Larson DE, Miller CA, Koboldt DC, Welch JS *et al*. Clonal evolution in relapsed acute myeloid leukaemia revealed by whole-genome sequencing. *Nature* 2012; **481**: 506–510.
  - 28 Lopez-Corral L, Gutiérrez NC, Vidriales MB, Mateos MV, Rasillo A, García-Sanz R *et al*. The progression from MGUS to smoldering myeloma and eventually to multiple myeloma involves a clonal expansion of genetically abnormal plasma cells. *Clin Cancer Res* 2011; **17**: 1692–1700.
  - 29 Hanamura I, Stewart JP, Huang Y, Zhan F, Santra M, Sawyer JR *et al*. Frequent gain of chromosome band 1q21 in plasma-cell dyscrasias detected by fluorescence *in situ* hybridization: incidence increases from MGUS to relapsed myeloma and is related to prognosis and disease progression following tandem stem-cell transplantation. *Blood* 2006; **108**: 1724–1732.
  - 30 Chiecchio L, Dagrada GP, Ibrahim AH, Dachs Cabanas E, Protheroe RK, Stockley DM *et al*. Timing of acquisition of deletion 13 in plasma cell dyscrasias is dependent on genetic context. *Haematologica* 2009; **94**: 1708–1713.
  - 31 Chapman MA, Lawrence MS, Keats JJ, Cibulskis K, Sougnez C, Schinzel AC *et al*. Initial genome sequencing and analysis of multiple myeloma. *Nature* 2011; **471**: 467–472.
  - 32 Morgan GJ, Walker BA, Davies FE. The genetic architecture of multiple myeloma. *Nat Rev Cancer* 2012; **12**: 335–348.
  - 33 Munshi NC, Anderson KC, Bergsagel PL, Shaughnessy J, Palumbo A, Durie B *et al*. International Myeloma Workshop Consensus Panel 2. Consensus recommendations for risk stratification in multiple myeloma: report of the International Myeloma Workshop Consensus Panel 2. *Blood* 2011; **117**: 4696–4700.

Supplementary Information accompanies the paper on the Leukemia website (<http://www.nature.com/leu>)